Photosensitizer doped zeolitic imidazolate framework-8 nanocomposites for combined antibacterial therapy to overcome methicillin-resistant Staphylococcus aureus (MRSA)

Photosensitizer doped zeolitic imidazolate framework-8 nanocomposites for combined antibacterial therapy to overcome methicillin-resistant *Staphylococcus aureus* (MRSA)

Juan Li,[†] Ashna Gopal,[‡] Sena Karaosmanoglu,[‡] Jiafu Lin,[†] Tasnim Munshi,[○] Wenjun Zhang,*[,§] Xianfeng Chen,*[, ‡] and Li Yan*[,†,§,‖]

[†] Antibiotics Research and Re-evaluation Key Laboratory of Sichuan Province, Sichuan Industrial Institute of Antibiotics (SIIA), Chengdu University, Chengdu, 610052, Sichuan, P.R. China.

[‡] School of Engineering, Institute for Bioengineering, The University of Edinburgh, King's Buildings, Mayfield Road, Edinburgh EH9 3JL, UK.

[§] Department of Materials Science and Engineering and Centre of Super Diamond & Advanced Film (COSDAF), City University of Hong Kong, Hong Kong SAR

[○] School of Chemistry, University of Lincoln, Brayford Pool, Lincoln, Lincolnshire, LN6 7TS, UK

Corresponding Authors

*Emails: tony_yan8@hotmail.com or tony.yan@monash.edu (L. Yan) Current Address: Monash Institute of Pharmaceutical Sciences, Monash University, Parkville, Victoria 3052, Australia, xianfeng.chen@oxon.org or Michael.Chen@ed.ac.uk (X. Chen) and apwjzh@cityu.edu.hk (W.J. Zhang)

The total number of words of the manuscript, including entire text from title page to figure legends: 5196

The number of words of the abstract: 109

The number of figures: 7

The number of tables: 0

Abstract

Antibiotics have played an important role in the treatment of bacteria related infections. However, the rapid emergence of multidrug-resistant bacteria and limited number of antibiotics available is a great challenge to humankind. To circumvent the use of antibiotics and hence, address this problem, we are proposing a photosensitizer-modified biodegradable zeolitic imidazolate framework-8 nanocomposite that can kill not only Gram-positive bacteria *Staphylococcus aureus*, but also methicillin-resistant *Staphylococcus aureus* with high efficacy. *In vivo* testing revealed that these nanocomposites are highly effective for *in vivo* wound disinfection with minimal side-effects. In conclusion, this photosensitizer-modified biodegradable nanocomposite could be very promising for a synergistic antibacterial therapy to overcome methicillin-resistant *Staphylococcus aureus* (MRSA).

Keywords: zeolitic imidazolate framework 8; photosensitizer; photodynamic therapy; antibacterial therapy

1. Introduction

Bacterial infection is one of the most prominent causes of serious diseases [1-3]. The wide range and biological variations of pathogenic microorganisms often lead to great challenges in antimicrobial treatment in clinical settings. With the discovery and development of antibiotics, the treatment of bacterial infection has been revolutionised[4-5]. However, long-term abuse and overdose of antibiotics have led to bacterial cells adversely modifying antibiotic molecules, thereby leading to the emergence of drug-resistant bacteria [6-7]. This, in turn, poses a serious public health threat that contributes to millions of severe infections and even thousands of deaths every year[8]. According to the World Health Organisation, more than 700,000 people die worldwide every year from antibiotic resistant infections and this figure is expected to rise to 10 million a year by 2050[9]. Although great efforts have been dedicated to creating new and more effective

antibiotics, the rate of antibiotic development is still far more behind the high evolution rate of pathogenic microorganisms. An example is methicillin-resistant *Staphylococcus aureus* (MRSA), which was first discovered in England and is considered as one of the most dangerous clinical pathogens (often known as 'superbugs') causing life-threatening diseases[10]. Thus, it is crucial that new antimicrobial agents and methods are developed to mitigate the persistent issue of drug tolerance. One potential solution is to use nanomaterials for the delivery of antimicrobial agents. The ability of nanomaterials to allow enhanced localization to bacteria as well as tunable interaction with bacteria upon surface modification with different charges, roughness, and functional groups can greatly improve therapeutic properties and efficiency[11]. Among nanomaterials, metal-organic frameworks (MOFs) have been developed for many biomedical applications[12-16]. MOFs are constructed using metal ions and organic linker molecules to form nanoporous materials with many advantages including high surface area, tunable pore size and porosity, high drug loading capacity, good biocompatibility, potential biodegradability, and greater flexibility in the selection of organic and inorganic components[17-19]. Therefore, several MOFs with different functionalities have been successfully designed for antibiotic and silver loading for increased antibacterial efficacy[20-22]. Liu and co-workers have reported the use of MIL-100 (Fe) MOFs as a nanocarrier to deliver the metabolic labelling molecule 3-azido-D-alanine for precise bacterial detection and fluorescence image-guided therapy[23]. Beyond these applications of using MOFs, we herein propose an integrated multifunctional nano MOF (NMOFs) system based on zeolitic imidazolate framework-8 (ZIF-8) for antibacterial applications (**Figure 1**). Photodynamic therapy (PDT) is widely utilized for biomedical applications including cancer therapy, wound healing and disinfection.[24-26] This technique makes use of light excitation to generate reactive oxygen species (ROS) to directly attack and kill pathogenic microorganisms[27-28]. The ROS reacts with diverse bioactive molecules in

pathogenic bacteria and its generation has been found to be very promising in the endeavour to solve the antibiotic resistance problem[29]. To achieve a nanocomposite capable of photodynamic therapy, the photosensitiser, Chlorin e6 (Ce6) was chosen because of its low dark toxicity and high efficacy. Furthermore, Ce6 was selected over other photosensitising drugs as it can be easily attached on the surface of the ZIF-8 via an intermediate conjugation step with APTES and then mixing with the ZIF-8 solution. Secondly, in our proposed hybrid structure, the Zn^{2+} ions act as a toxin for the inhibition of bacterial growth[30]. Third, the nanoparticles possess a rough surface which has been demonstrated to drastically influence the interaction with bacterial cells, thereby achieving high antibacterial efficacy[31-33]. Finally, the soft-template based NMOFs are pH-sensitive and easiliy decompose in a weak acid environment compared to other nanocomposites such as silica and zinc oxides nanoparticles.

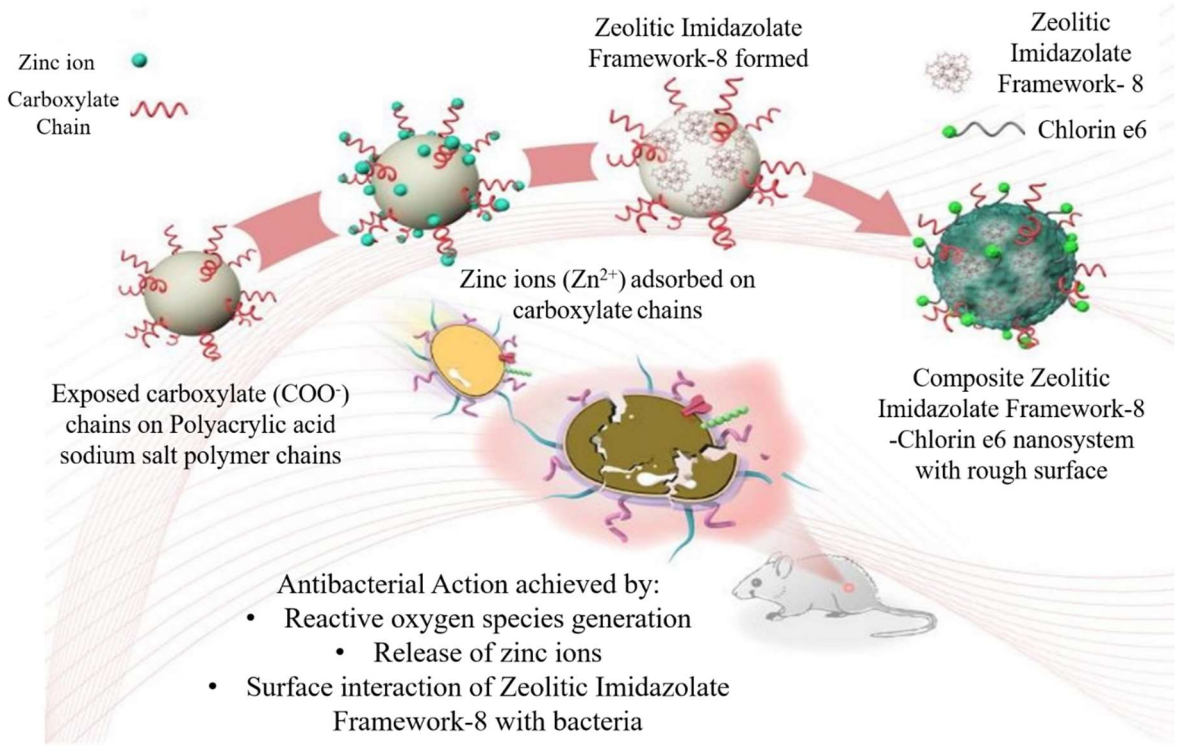

Figure 1. Schematic illustration of Ce6 doped ZIF-8 nanoparticles fabrication and their use for photo-inspired disinfection.

2. EXPERIMENTAL SECTION

2.1 Chemicals and Characterization. 1-Ethyl-3-(3-dimethylaminopropyl) carbodiimide (EDC), 2-methylimidazole (linker) and 1, 3-diphenylisobenzofuran (DPBF) were purchased from Damas-beta. Zinc nitrate hexahydrate ($Zn(NO_3)_2 \cdot 6H_2O$) and poly(acrylic acid, sodium salt) (PAAS) were from Strem and Sigma-Aldrich, respectively. Methyl alcohol, ethyl alcohol, isopropyl alcohol and absolute ethyl alcohol, were purchased from General-Reagent, China. (3-aminopropyl) triethoxysilane (APTES) and Chlorin e6 (Ce6) were ordered from J&K and Frontier Scientific, respectively. Transmission electron microscopy (TEM) images were taken on a Tecnai G2 F20 S-TWIN. The UV−VIS absorption spectrum was determined with a UV-1900PC UV−visible spectrophotometer. Powder X-ray diffraction (XRD) patterns, Fourier transform infrared spectroscopy (FT-IR) and X-ray photoelectron spectroscopy (XPS) were recorded using a BRUKER D8 instrument with Cu Kα radiation, Nicolet IS10 and Thermo escalab 250Xi, respectively. The L13152 Invitrogen™ Molecular Probes™ LIVE/DEAD® BacLight Bacterial Viability Kit was obtained from Thermo Fisher Scientific.

2.2 Preparation of APTES Conjugated Ce6. 1 mg of Ce6 and 20 μL of APTES were added to 1 mL of ethyl alcohol in the presence of EDC as a catalyst and magnetically stirred for 24 h at room temperature.

2.3 Preparation of ZIF-8 and Ce6 doped ZIF-8. First, 50 μL of 200 μg/mL PAAS were added to 1.5 mL of H_2O, then 6 mL of isopropyl alcohol was added in a dropwise manner. 0.1M Zn^{2+} solution was prepared by dissolving $Zn(NO_3)_2 \cdot 6H_2O$ in methyl alcohol and 1.25 mL of the 0.1 M Zn^{2+} was quickly added to the liquid mixture and stirred for 5 min at room temperature. 2.5 mL of 20 mg/mL 2-methylimidazole dissolved in methyl alcohol was then injected into the mixture and kept stirring for 4 h at 60°C. The solution was subsequently cooled and precipitated by centrifugation at 6000 rpm for 10 min. The resulting solid was washed with absolute ethyl alcohol and water thrice. The sediment was then dispersed into 5 mL of 50% ethyl alcohol. Next, the APTES conjugated Ce6 was added to the solution and kept stirring for an additional

24 h. After the reaction, the product was washed with ethyl alcohol and water thrice and then dried in a vacuum to yield Ce6 doped ZIF-8.

2.4 Singlet Oxygen Generation Ability Analysis. 2.82 mL of 0.05 mg/mL DPBF solution in dimethyl sulfoxide (DMSO) was added into a quartz colorimetric dish. 0.18 mL of free Ce6 or Ce6 doped ZIF-8 containing 900 ng of Ce6 was added to different individual dishes. The dishes were then irradiated with a 650 nm LED lamp. After irradiation, the absorbance of the sample in each dish was measured at 410 nm using a UV-1900PC UV−visible spectrophotometer.

2.5 Antibacterial Test. *Staphylococcus aureus* (*S. aureus*) and MRSA were chosen as bacterial models to evaluate the antibacterial activity. The bacterial concentration in Lysogeny broth (LB) was maintained at about 10^6 CFU mL^{-1} and cultured at 37ºC in an incubator-shaker. Corning 96-well plates were used for this test. Four pre-determined concentrations of nanoparticles were prepared in milli-Q water and these were added to the bacterial suspension in a 1:1 ratio and then incubated. For the groups being treated with light, the Corning 96-well plates were exposed to 650 nm LED light for 30 minutes at an intensity of 150 (100x LUX) before incubation at 37 ºC for 12 h. The bacterial inhibition growth curve was determined by measuring the optical density at 600 nm at 2 h time intervals over the 12-h period.

2.6 Live-Dead Imaging. The antibacterial effect of Ce6-doped ZIF-8 nanoparticles and LED light irradiation were demonstrated using Live/Dead Imaging. *Staphylococcus Aureus* was used as the model bacteria. Four treatment groups were considered namely, bacteria without light irradiation (A), bacteria with light irradiation (B), nanoparticles treated with bacteria but without light irradiation (C) and nanoparticles treated with bacteria with light irradiation (D). 10 µL from a *Staphylococcus Aureus* (USA300) stock was cultured overnight on LB agar at 37℃ for 18 h. A single colony was then inoculated in liquid LB media and grown overnight at 37 °C with shaking at 200 rpm. The overnight culture was then diluted (1:100) and the sample incubated until an optical density of ~0.5 at 600 nm was reached. PBS was then used to wash the culture by centrifugation at 5000 rpm for 5 minutes at 4 °C and resuspension. Fresh liquid

media was added to the bacteria and then serially diluted to adjust the optical density to 0.05 (~10^6 CFU mL^{-1}). A stock solution of the Ce6-doped ZIF-8 nanoparticles dispersed in milli-Q water was prepared at a concentration of 1 mg/mL. Then, a 5 mL solution with a concentration of 22.2 μg/mL from this stock solution was prepared and sonicated for 20 mins for an even nanoparticle dispersion. 1 mL of this solution was added to 1 mL of the bacterial culture (for conditions C and D) in a sterile 6-well plate. The bacterial suspension for conditions A and B were left untreated and 1 mL of PBS was added as a control. The plate was then incubated at 37℃ for 2 hours in the dark with shaking. After 2 hours, the wells containing bacteria from conditions B and D were exposed to a 650 nm LED light source for 30 minutes placed at a vertical height of 22 cm from the plate. The plate was then further incubated for 2 hours at 37℃ with shaking. After incubation, a 1:1000 dilution was carried out with each of the four samples and 100 μL of the diluted solution was plated for CFU determination. The remaining solution in each well was transferred into 2 mL Eppendorf tubes, washed thrice with PBS by centrifugation at 15000 rpm for 5 mins and then re-suspended in 500 μL of PBS. The four samples were then stained by adding an equal amount of PI/Syto9 dye mixture prepared as per the manufacturer's instructions. The stained bacterial suspensions were then incubated in the dark for 15 minutes. To remove excess dye, each sample was washed with PBS thrice by centrifugation at 20000 rpm for 5 mins and then finally resuspended in 200 μL of PBS. 20 μL of each of this stained bacterial suspension was trapped between a slide and a 25 mm diameter round coverslip. The edges of the coverslip were sealed, and the samples observed in a Zeiss LSM 880 with Fast Airyscan confocal microscope.

2.7 Animal Wound Infection Model and Histological Analysis. All the procedures were carried out in accordance with the guidelines issued by Chengdu University and Sichuan Province. All the experiments were approved by the Animal Ethics Committee of Chengdu University. Four groups of mice were randomly divided. A wound of about 6 mm^2 was

developed at the dorsal side of each mouse. After 24 h, the wounds were infected with *S. aureus* and then treated with the Ce6 doped ZIF-8 nanoparticles. The light treated group of mice was exposed to 650 nm LED light for 30 mins. At day 17, all mice were sacrificed. The heart, liver, spleen, lung, kidney, and wound were harvested and the tissues fixed in a 10% formalin solution, embedded in paraffin, sectioned, and stained. All the samples were subsequently processed for hematoxylin and eosin (H&E) staining.

3. RESULTS AND DISCUSSION

Nanoscale ZIF-8 was fabricated using poly(acrylic acid sodium salt) (PAAS) nanosphere as a soft template.[34-35] Since Zn^{2+} has a higher affinity towards the $–COO^-$ group in the PAAS polymer chain, it was absorbed on the PAAS and thus, replaced the Na^+. Then, 2-methylimidazole (2-MIMs) was added and reacted with the Zn^{2+} on the surface to form ZIF-8 nanocrystal on the PAA nanosphere. Next, (3-aminopropyl) triethoxysilane (APTES) conjugated Ce6 was reacted with the nanocomposite for drug conjugation. The ZIF-8 nanocomposite has a diameter of approximately 50-90 nm and (**Figure 2** and Figure S1) the Ce6 loading in the nanocomposite is 4.5 wt% (Figure 2 and Figure S1). As illustrated in **Figure 3A**, the fabricated nanocomposite has XRD peaks identical to ZIF-8, confirming successful formation of ZIF-8 crystal structure. The Fourier transform infrared (FT-IR) spectrum of the nanocomposite contains Ce6 peaks, establishing the successful conjugation of Ce6 (Figure 3B). In addition, the X-ray photoelectron spectroscopy (XPS) confirms the existence of Zn and Si elements in the nanoparticles with a weight atomic ratio of 8.58% and 4.11%, respectively. (Figure 3C-E and Table S1)

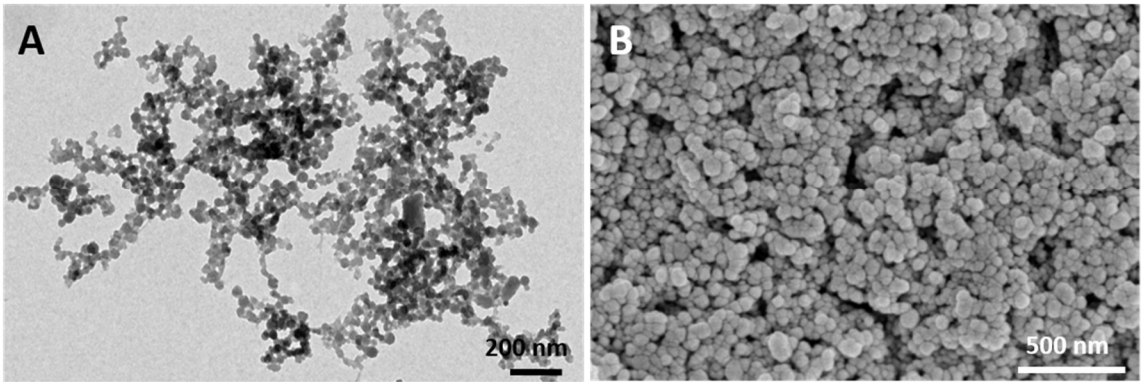

Figure 2. Characterisation of Ce6 doped ZIF-8 nanoparticles: A. TEM image and B. SEM image.

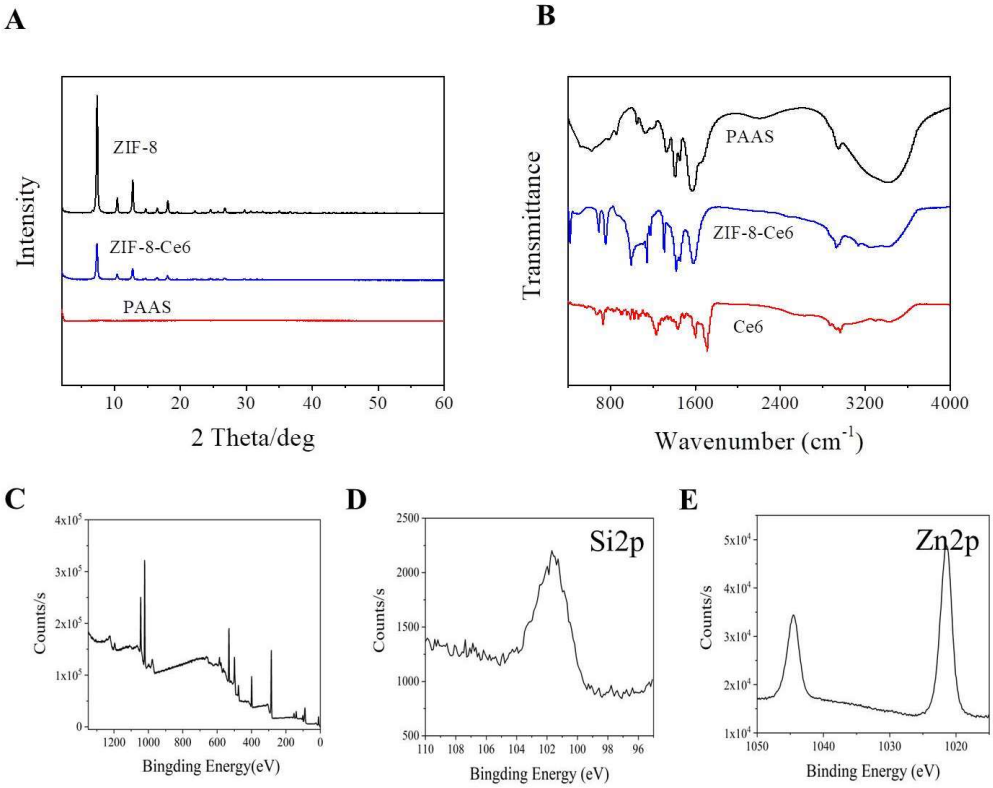

Figure 3 A. Powder X-Ray diffraction pattern, B. Fourier transform infrared spectroscopy and C. XPS analysis of Ce6 doped ZIF-8 nanoparticles.

Next, the optical properties of the Ce6 doped ZIF-8 were evaluated. **Figure 4**A shows the absorbance spectra of Ce6 doped ZIF-8 nanocomposite and free Ce6 molecules, it is apparent that the spectra are similar but with a shift in absorbance of the peaks. We then investigated the photo-stability of the Ce6 doped ZIF-8 when exposed to light (Figure 4B and Figure S2), it was found that the absorbance intensity of free Ce6 molecules dramatically decreases after a short period of light exposure. In contrast, the absorbance intensity of Ce6 doped ZIF-8

nanocomposite is much more stable. Next, a fluorescence probe, 1, 3-diphenylisobenzofuran (DPBF), was used to detect singlet oxygen molecules and study the ROS generation capacity of the Ce6 doped ZIF-8 nanoparticles. Under 650 nm LED light irradiation, both free Ce6 molecules and Ce6 doped ZIF-8 can effectively generate singlet oxygen (Figure 4C). To further study the photo-stability of the Ce6 doped ZIF-8 nanocomposites, their ROS generation capacity was investigated after light exposure. Both Ce6 doped ZIF-8 and Ce6 molecules were initially exposed to 650 nm LED light for 30 minutes and then the formation of ROS from each material was studied. As presented in Figure 4D, free Ce6 molecules lose the majority of their ROS generation capacity after light exposure as indicated by the small decrease in rate of the absorbance of DPBF, while the Ce6 doped ZIF-8 can still generate ROS, thereby resulting in a substantial decrease of the absorbance of DPBF. Next, we tested the biodegradability of fabricated Ce6 doped nanoscale ZIF-8 in a weak acid environment. As shown in Figure S3, the nanocomposite is biodegradable in a weak acid environment and loses its whole structure within 6 hours in a pH 5 environment.

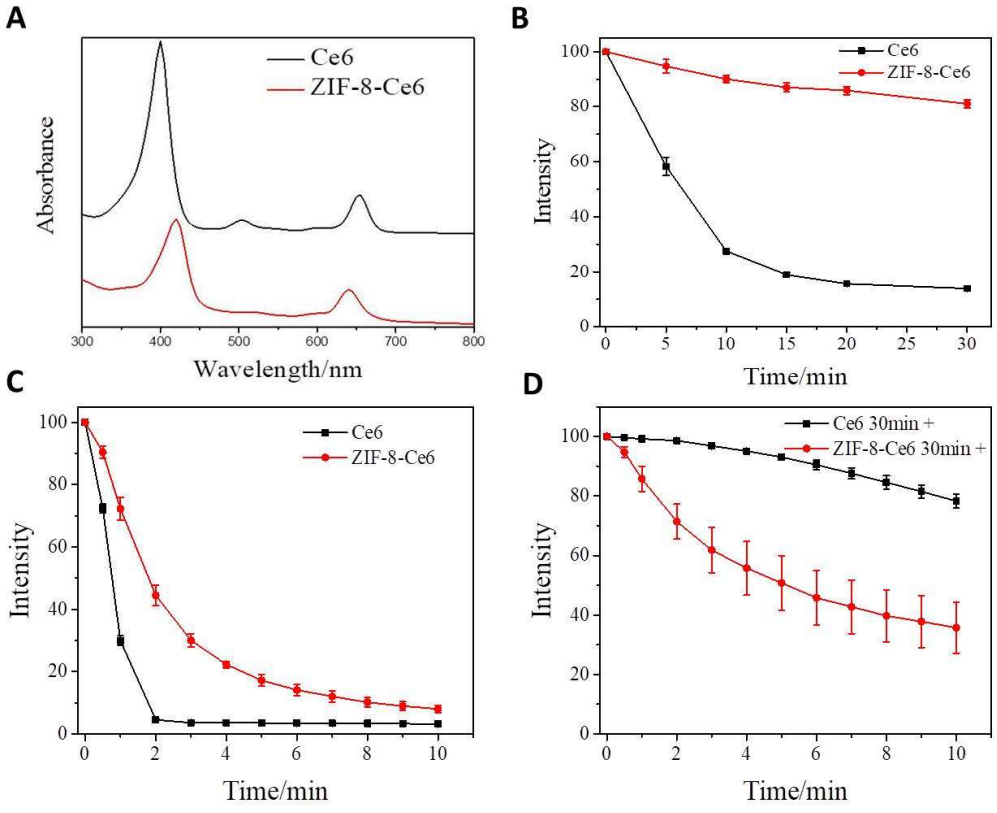

Figure 4. Optical properties and singlet oxygen generation capacity of Ce6 doped ZIF-8 nanoparticles. A. Absorption spectra of Ce6 doped ZIF-8 and free Ce6 molecules. B. Normalized 400 nm absorbance intensity change of Ce6 doped silica and free Ce6 caused by 650 nm LED irradiation. C-D. Absorbance spectra of DPBF with the addition of Ce6 doped silica and free Ce6 under LED illumination. (C) Degradation in intensity when DPBF added with Ce6 doped silica and free Ce6, (D) Degradation in intensity when Ce6 doped silica and free Ce6 were illuminated under 650 nm LED light for 30 min before addition of DPBF. Data in B-D are expressed as mean ± s.d. (indicated by error bars), based on values obtained from three replicates (n=3).

The antibacterial performance of Ce6 doped ZIF-8 was subsequently analyzed with *S. aureus* and MRSA as model bacteria (Figure S4 and **Figure 5**). The growth of bacteria in liquid media was monitored by measuring the optical density of Luria-Bertani (LB) broth at a wavelength of 600 nm. At first, the influence of light irradiation on bacterial growth was excluded by comparing the growth of bacteria with and without light illumination. It was found that the bacterial growth with and without light illumination was nearly identical, suggesting that the light at the used power does not inhibit bacteria growth. At a concentration of 200 μg/mL, the Ce6 doped ZIF-8 nanoparticles could effectively inhibit the growth of *S. aureus* and MRSA irrespective of light illumination. This indicates that the Ce6 doped ZIF-8 nanoparticles are toxic to bacteria; the toxicity originates from the Zn^{2+} ions within the material, as Ce6 cannot kill bacteria in the absence of light illumination. When the concentration was decreased to 66.7 μg/mL, the Ce6 doped ZIF-8 nanoparticles partially inhibited the growth of bacteria in the absence of light irradiation. In comparison, Ce6 doped ZIF-8 nanoparticles at the same concentration could effectively inhibit the growth of both MRSA and *S. aureus* upon light irradiation. This demonstrates that the photo-toxicity of the Ce6 doped ZIF-8 is also responsible for bacterial growth inhibition. To confirm this observation, we further dropped the concentration of the Ce6 doped ZIF-8 nanocomposite to 22.2 and 7.4 μg/mL and found that the Ce6 doped ZIF-8 nanoparticles were still able to completely inhibit *S. aureus* and MRSA growth in the presence of LED light. This finding was also confirmed when the plate count method was used (Figure S5 and Figure S6). Results from a statistical t-test revealed a p-value

of <<0.05 which showed a significant difference between the ZIF-Ce6 nanoparticles and light group and any other group at the 12 h time point for all 4 tested concentrations. Overall, the Ce6 doped ZIF-8 nanoparticles exhibited excellent light-induced antibacterial performance.

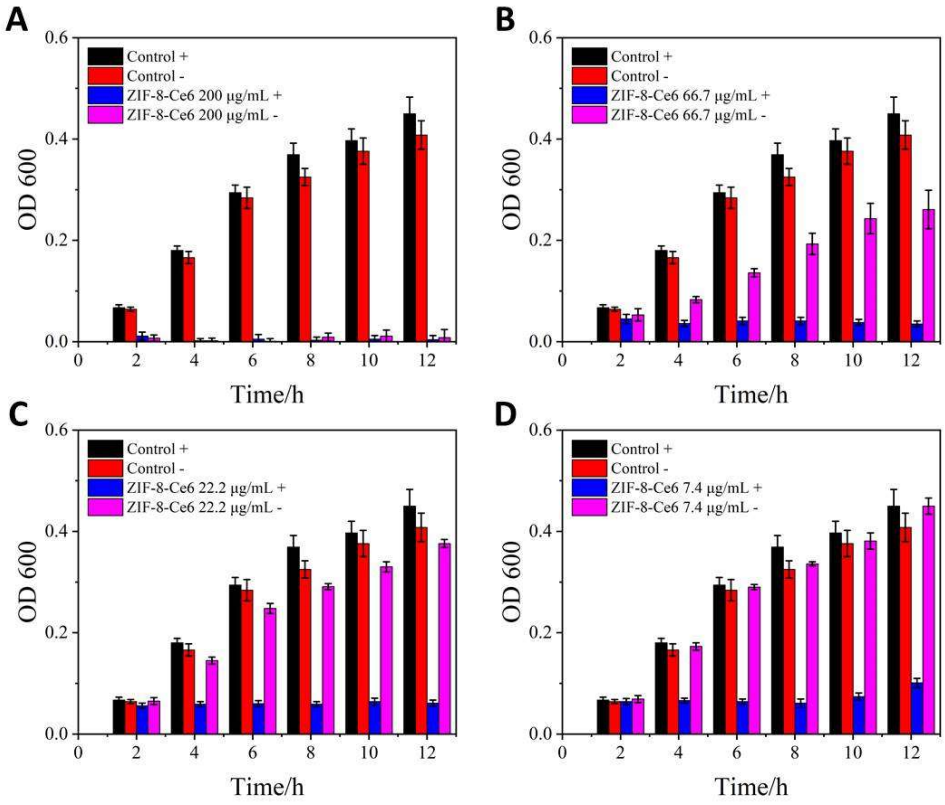

Figure 5. Anti-MRSA performance of Ce6 doped ZIF-8 with different concentrations: A. 200 μg/mL, B. 66.7 μg/mL, C. 22.2 μg/mL and D. 7.4 μg/mL. Control means only LB added. "+" indicates with light illumination; "-" indicates without light illumination. All data are expressed as mean ± s.d. (indicated by error bars), based on values obtained from six biological replicates (n=6).

After demonstrating the antibacterial ability of Ce6-doped ZIF-8 nanoparticles by measuring the optical density and counting the CFU number of bacteria, we continued this investigation using confocal fluorescence microscopy imaging. We performed Live/Dead bacterial staining using the L13152 Invitrogen™ Molecular Probes™ BacLight™ Bacterial Viability Kit. The Syto9 dye stains bacteria with both intact membranes and damaged membranes while the propidium iodide dye penetrates only the bacteria with damaged membranes. As evidenced by the confocal images in **Figure 6**, a low concentration of Ce6-doped ZIF-8 nanoparticles (22.2 μg/mL) alone is not enough to kill all bacterial cells; however, if bacteria are exposed to both

nanoparticles at the same concentration and light irradiation, nearly all bacteria are killed. This is in line with the above results obtained by CFU plating and optical density measurements. The synergistic effect shown in these experiments demonstrates the potent efficacy of the proposed combined therapy and implies that nanoparticles at very low concentrations can still yield effective antibacterial efficiency.

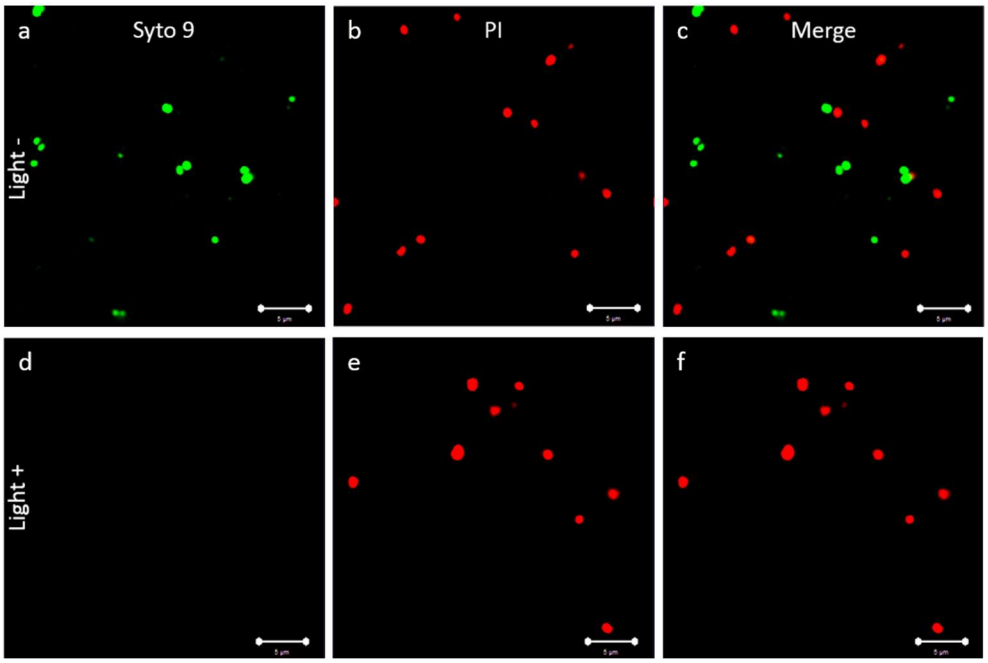

Figure 6. Live/dead staining of *S. aureus* treated with Ce6-doped ZIF-8 nanoparticles in the absence of light (Light -) (a-c) and presence of light irradiation (light +) (d-f). Scale bars indicate 5 μm. The concentration of Ce6-doped ZIF-8 nanoparticles used for imaging was 22.2 μg/mL.

Finally, it is important to determine if this technique could be potentially used in clinical applications. Thus, the *in vivo* anti-infection performance of Ce6 doped ZIF-8 nanoparticles was evaluated using a Balb/c mouse model. A wound was created on the back of mice followed by infection with *S. aureus* bacteria. (**Figure 7**) The mice were then randomly divided into four groups. One group of mice was treated with free Ce6 molecules and irradiated with light. Two groups of mice were treated with Ce6 doped ZIF-8 nanoparticles (one with light irradiation and the other without light irradiation). Another group of mice were used as a control and not subjected to any treatment. Figure 7A shows the digital images of wounds for each of the

different treatment conditions. A clear difference in wound morphology after treatment was observed. It is apparent that the wounds treated by the Ce6 doped ZIF-8 nanoparticles with light irradiation show a better recovery pattern than other groups. Wounds like the ones introduced in this experiment have a general tendency to be alkaline and slowly turn acidic as wound healing is initiated.[36] As the ZIF-8-Ce6 nanocomposites are responsive to acidic pH, their dissociation within the wound environment could enhance their antibacterial function while being finally cleared. Haemotoxylin and Eosin (H&E) analysis of wound harvested from mice treated with both Ce6 doped ZIF-8 and light irradiation reveals a complete and intact skin structure. In addition, no obvious abnormality was found in the major organs of the mice treated with the Ce6 doped ZIF-8 nanoparticles and light irradiation.(Figure S7) During the whole experimental period, no obvious change in body weight was found in all groups (Figure 7B). Collectively, these observations demonstrate the robust wound healing efficiency and good biocompatibility of the synthesized Ce6-doped ZIF-8 nanoparticles.

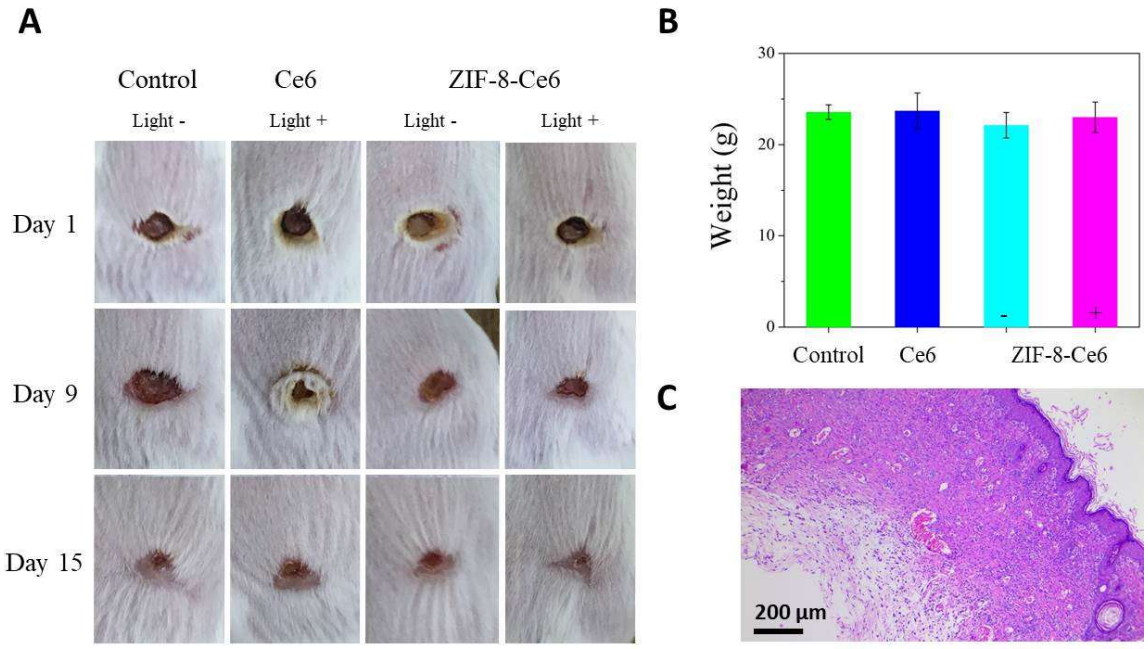

Figure 7. *In vivo* antibacterial evaluation of *S. aureus* infected wound treated with Ce6 doped ZIF-8. A. Digital images of *S. aureus* infected wound treated with different drug formations. B. Body weight of mice treated in different groups. Data are expressed as mean ± s.d. (indicated by error bars). C. Haematoxylin and Eosin stain of *S. aureus* infected skin tissue sections treated with Ce6 doped rough silica with light irradiation.

4. Conclusion

In conclusion, our study illustrates a strategy for the synthesis of Ce6 doped ZIF-8 nanoparticles for enhanced antibacterial applications, with a strong potential for killing bacteria with multi-drug resistance. The conjugation of Ce6 to ZIF-8 nanoparticles could significantly improve the photostability and ROS generation capacity of free Ce6 molecules. Our *in vitro* testing and live/dead imaging demonstrates the excellent synergistic therapeutic efficacy of the Ce6-doped ZIF-8 nanoparticles against *S. aureus* and MRSA. The *in vivo* wound healing studies on *S. aureus* infected mice further confirmed the highly effective antibacterial performance and good biocompatibility of the nanoparticles and thus, warrants their future applications in clinical settings.

Declaration of Interest

-

Appendix A. Supplementary data

Supplementary material (SEM images, time-dependent morphology and absorbance changes, bacterial colony-forming units, hematoxylin and eosin stain images) related to this article can be found, in the online version, at doi:

ACKNOWLEDGMENTS

The authors acknowledge the support provided from National Natural Science Foundation of China (No. 81803480), General Research Fund of Hong Kong (CityU Grant Nos. 11338516 and 11306717), the Royal Society Research Grant Scheme RG150564 and the Chengdu University (Nos. 2081916010 and ARRLKF16-05).
J. Li and A. Gopal contributed equally to this work.

REFERENCES

1. Li, M.; Sultanbawa, Y.; Xu, Z. P.; Gu, W.; Chen, W.; Liu, J.; Qian, G., High and long-term antibacterial activity against Escherichia coli via synergy between the antibiotic penicillin G and its carrier ZnAl layered double hydroxide. *Colloids Surf. B Biointerfaces* **2019,** *174*, 435-442. DOI: 10.1016/j.colsurfb.2018.11.035.
2. Chen, W.; Zhang, B.; Mahony, T.; Gu, W.; Rolfe, B.; Xu, Z. P., Efficient and Durable Vaccine against Intimin beta of Diarrheagenic E. Coli Induced by Clay Nanoparticles. *Small* **2016,** *12* (12), 1627-39. DOI: 10.1002/smll.201503359.

3. Zhang, M.; Wang, P.; Sun, H.; Wang, Z., Superhydrophobic surface with hierarchical architecture and bimetallic composition for enhanced antibacterial activity. *ACS Appl. Mater. Interfaces* **2014,** *6* (24), 22108-15. DOI: 10.1021/am505490w.
4. Li, Y.; Zhao, Z.; Zhang, J.; Kwok, R. T. K.; Xie, S.; Tang, R.; Jia, Y.; Yang, J.; Wang, L.; Lam, J. W. Y.; Zheng, W.; Jiang, X.; Tang, B. Z., A Bifunctional Aggregation-Induced Emission Luminogen for Monitoring and Killing of Multidrug-Resistant Bacteria. *Adv. Funct. Mater.* **2018,** *28* (42), 1804632. DOI: 10.1002/adfm.201804632.
5. Klein, E. Y.; Van Boeckel, T. P.; Martinez, E. M.; Pant, S.; Gandra, S.; Levin, S. A.; Goossens, H.; Laxminarayan, R., Global increase and geographic convergence in antibiotic consumption between 2000 and 2015. *Proc. Natl. Acad. Sci.* **2018,** *115* (15), E3463. DOI: 10.1073/pnas.1717295115.
6. Li, X.; Bai, H.; Yang, Y.; Yoon, J.; Wang, S.; Zhang, X., Supramolecular Antibacterial Materials for Combatting Antibiotic Resistance. *Adv. Mater.* **2019,** *31* (5), 1805092. DOI: 10.1002/adma.201805092.
7. Dai, X.; Zhao, Y.; Yu, Y.; Chen, X.; Wei, X.; Zhang, X.; Li, C., All-in-one NIR-activated nanoplatforms for enhanced bacterial biofilm eradication. *Nanoscale* **2018,** *10* (39), 18520-18530. DOI: 10.1039/C8NR04748K.
8. Linklater, D. P.; De Volder, M.; Baulin, V. A.; Werner, M.; Jessl, S.; Golozar, M.; Maggini, L.; Rubanov, S.; Hanssen, E.; Juodkazis, S.; Ivanova, E. P., High Aspect Ratio Nanostructures Kill Bacteria via Storage and Release of Mechanical Energy. *ACS Nano* **2018,** *12* (7), 6657-6667. DOI: 10.1021/acsnano.8b01665.
9. Tagliabue, A.; Rappuoli, R., Changing Priorities in Vaccinology: Antibiotic Resistance Moving to the Top. *Frontiers immunol.* **2018,** *9*, 1068-1068. DOI: 10.3389/fimmu.2018.01068.
10. Hu, D.; Li, H.; Wang, B.; Ye, Z.; Lei, W.; Jia, F.; Jin, Q.; Ren, K.-F.; Ji, J., Surface-Adaptive Gold Nanoparticles with Effective Adherence and Enhanced Photothermal Ablation of Methicillin-Resistant Staphylococcus aureus Biofilm. *ACS Nano* **2017,** *11* (9), 9330-9339. DOI: 10.1021/acsnano.7b04731.
11. Armentano, I.; Arciola, C. R.; Fortunati, E.; Ferrari, D.; Mattioli, S.; Amoroso, C. F.; Rizzo, J.; Kenny, J. M.; Imbriani, M.; Visai, L., The interaction of bacteria with engineered nanostructured polymeric materials: a review. *TheScientificWorldJournal* **2014,** *2014*, 410423-410423. DOI: 10.1155/2014/410423.
12. Chao, Y.; Liang, C.; Yang, Y.; Wang, G.; Maiti, D.; Tian, L.; Wang, F.; Pan, W.; Wu, S.; Yang, K.; Liu, Z., Highly Effective Radioisotope Cancer Therapy with a Non-Therapeutic Isotope Delivered and Sensitized by Nanoscale Coordination Polymers. *ACS Nano* **2018,** *12* (8), 7519-7528. DOI: 10.1021/acsnano.8b02400.
13. Yang, Y.; Xu, L.; Zhu, W.; Feng, L.; Liu, J.; Chen, Q.; Dong, Z.; Zhao, J.; Liu, Z.; Chen, M., One-pot synthesis of pH-responsive charge-switchable PEGylated nanoscale coordination polymers for improved cancer therapy. *Biomaterials* **2018,** *156*, 121-133. DOI: https://doi.org/10.1016/j.biomaterials.2017.11.038.
14. Liu, Y. L.; Tang, Z. Y., Multifunctional Nanoparticle@MOF Core-Shell Nanostructures. *Adv. Mater.* **2013,** *25* (40), 5819-5825. DOI: 10.1002/adma.201302781.
15. Li, Y. T.; Tang, J. L.; He, L. C.; Liu, Y.; Liu, Y. L.; Chen, C. Y.; Tang, Z. Y., Core-Shell Upconversion Nanoparticle@Metal-Organic Framework Nanoprobes for Luminescent/Magnetic Dual-Mode Targeted Imaging. *Adv. Mater.* **2015,** *27* (27), 4075-4080. DOI: 10.1002/adma.201501779.
16. Fan, X.; Yang, F.; Nie, C. X.; Yang, Y.; Ji, H. F.; He, C.; Cheng, C.; Zhao, C. S., Mussel-Inspired Synthesis of NIR-Responsive and Biocompatible Ag-Graphene 2D Nanoagents for Versatile Bacterial Disinfections. *ACS Appl. Mater. Interfaces* **2018,** *10* (1), 296-307. DOI: 10.1021/acsami.7b16283.

17. Furukawa, H.; Cordova, K. E.; O'Keeffe, M.; Yaghi, O. M., The Chemistry and Applications of Metal-Organic Frameworks. *Science* **2013,** *341* (6149), 1230444. DOI: 10.1126/science.1230444.
18. Zhao, M.; Yuan, K.; Wang, Y.; Li, G.; Guo, J.; Gu, L.; Hu, W.; Zhao, H.; Tang, Z., Metal–organic frameworks as selectivity regulators for hydrogenation reactions. *Nature* **2016,** *539*, 76. DOI: 10.1038/nature19763
https://www.nature.com/articles/nature19763#supplementary-information.
19. Lu, K.; Aung, T.; Guo, N.; Weichselbaum, R.; Lin, W., Nanoscale Metal–Organic Frameworks for Therapeutic, Imaging, and Sensing Applications. *Adv. Mater.* **2018,** *30* (37), 1707634. DOI: 10.1002/adma.201707634.
20. Lin, S.; Liu, X.; Tan, L.; Cui, Z.; Yang, X.; Yeung, K. W. K.; Pan, H.; Wu, S., Porous Iron-Carboxylate Metal–Organic Framework: A Novel Bioplatform with Sustained Antibacterial Efficacy and Nontoxicity. *ACS Appl. Mater. Interfaces* **2017,** *9* (22), 19248-19257. DOI: 10.1021/acsami.7b04810.
21. Yuan, Y.; Wu, H.; Lu, H.; Zheng, Y.; Ying, J. Y.; Zhang, Y., ZIF nano-dagger coated gauze for antibiotic-free wound dressing. *Chem. Commun.* **2019,** *55* (5), 699-702. DOI: 10.1039/C8CC08568D.
22. Song, Z.; Wu, Y.; Cao, Q.; Wang, H.; Wang, X.; Han, H., pH-Responsive, Light-Triggered on-Demand Antibiotic Release from Functional Metal–Organic Framework for Bacterial Infection Combination Therapy. *Adv. Funct. Mater.* **2018,** *28* (23), 1800011. DOI: 10.1002/adfm.201800011.
23. Mao, D.; Hu, F.; Kenry; Ji, S.; Wu, W.; Ding, D.; Kong, D.; Liu, B., Metal–Organic-Framework-Assisted In Vivo Bacterial Metabolic Labeling and Precise Antibacterial Therapy. *Adv. Mater.* **2018,** *30* (18), 1706831. DOI: 10.1002/adma.201706831.
24. Cui, D.; Huang, J. G.; Zhen, X.; Li, J. C.; Jiang, Y. Y.; Pu, K. Y., A Semiconducting Polymer Nano-prodrug for Hypoxia-Activated Photodynamic Cancer Therapy. *Angew. Chem. Inter. Ed.* **2019,** *58* (18), 5920-5924. DOI: 10.1002/anie.201814730.
25. Ng, C. W.; Li, J. C.; Pu, K. Y., Recent Progresses in Phototherapy-Synergized Cancer Immunotherapy. *Adv. Funct. Mater.* **2018,** *28* (46). DOI: ARTN 1804688
10.1002/adfm.201804688.
26. Cui, D.; Xie, C.; Li, J. C.; Lyu, Y.; Pu, K. Y., Semiconducting Photosensitizer-Incorporated Copolymers as Near-Infrared Afterglow Nanoagents for Tumor Imaging. *Adv. Healthcare Mater.* **2018,** *7* (18). DOI:10.1002/adhm.201800329.
27. Ge, J.; Lan, M.; Zhou, B.; Liu, W.; Guo, L.; Wang, H.; Jia, Q.; Niu, G.; Huang, X.; Zhou, H.; Meng, X.; Wang, P.; Lee, C.-S.; Zhang, W.; Han, X., A graphene quantum dot photodynamic therapy agent with high singlet oxygen generation. *Nature Communications* **2014,** *5*, 4596. DOI: 10.1038/ncomms5596
28. Chen, *X. C.*; Zhang, *W.*, Diamond nanostructures for drug delivery, bioimaging, and biosensing. *Chem. Soc. Rev.* **2017,** *46* (3), 27. DOI: 10.1039/C6CS00109B.
29. Ristic, B. Z.; Milenkovic, M. M.; Dakic, I. R.; Todorovic-Markovic, B. M.; Milosavljevic, M. S.; Budimir, M. D.; Paunovic, V. G.; Dramicanin, M. D.; Markovic, Z. M.; Trajkovic, V. S., Photodynamic antibacterial effect of graphene quantum dots. *Biomaterials* **2014,** *35* (15), 4428-4435. DOI: https://doi.org/10.1016/j.biomaterials.2014.02.014.
30. Li, M.; Sultanbawa, Y.; Xu, Z. P.; Gu, W.; Chen, W.; Liu, J.; Qian, G., High and long-term antibacterial activity against Escherichia coli via synergy between the antibiotic penicillin G and its carrier ZnAl layered double hydroxide. *Colloids Surf. B: Biointerfaces* **2019,** *174*, 435-442. DOI: https://doi.org/10.1016/j.colsurfb.2018.11.035.
31. Song, H.; Ahmad Nor, Y.; Yu, M.; Yang, Y.; Zhang, J.; Zhang, H.; Xu, C.; Mitter, N.; Yu, C., Silica Nanopollens Enhance Adhesion for Long-Term Bacterial Inhibition. *J. Am. Chem. Soc.* **2016,** *138* (20), 6455-6462. DOI: 10.1021/jacs.6b00243.

32. Yue, Q.; Zhang, Y.; Jiang, Y.; Li, J.; Zhang, H.; Yu, C.; Elzatahry, A. A.; Alghamdi, A.; Deng, Y.; Zhao, D., Nanoengineering of Core–Shell Magnetic Mesoporous Microspheres with Tunable Surface Roughness. *J. Am. Chem. Soc.* **2017,** *139* (13), 4954-4961. DOI: 10.1021/jacs.7b01464.
33. Xu, R.; Huang, L.; Wei, W.; Chen, X.; Zhang, X.; Zhang, X., Real-time imaging and tracking of ultrastable organic dye nanoparticles in living cells. *Biomaterials* **2016,** *93*, 38-47. DOI: https://doi.org/10.1016/j.biomaterials.2016.03.045.
34. Yan, L.; Chen, X. F.; Wane, Z. G.; Zhang, X. J.; Zhu, X. Y.; Zhou, M. J.; Chen, W.; Huang, L. B.; Roy, V. A. L.; Yu, P. K. N.; Zhu, G. Y.; Zhang, W. J., Size Controllable and Surface Tunable Zeolitic Imidazolate Framework-8-Poly(acrylic acid sodium salt) Nanocomposites for pH Responsive Drug Release and Enhanced in Vivo Cancer Treatment. *ACS Appl. Mater. Interfaces* **2017,** *9* (38), 32990-33000. DOI: 10.1021/acsami.7b10064.
35. Ren, H.; Zhang, L. Y.; An, J. P.; Wang, T. T.; Li, L.; Si, X. Y.; He, L.; Wu, X. T.; Wang, C. G.; Su, Z. M., Polyacrylic acid@zeolitic imidazolate framework-8 nanoparticles with ultrahigh drug loading capability for pH-sensitive drug release. *Chem. Commun.* **2014,** *50* (8), 1000-1002. DOI: 10.1039/c3cc47666a.
36. Basavraj, S. N.; Namdev, M. S.; Bharat, W.; Sohan, S., Acidic Environment and Wound Healing: A Review. *Wounds.* **2015**, 27 (1), 5-11.